2012 American Control Conference
Fairmont Queen Elizabeth, Montréal, Canada
June 27-June 29, 2012

Next-Generation Wafer Stage Motion Control: Connecting System Identification and Robust Control

Tom Oomen, Robbert van Herpen, Sander Quist, Marc van de Wal, Okko Bosgra, Maarten Steinbuch

Abstract— **Next-generation precision motion systems are lightweight to meet stringent requirements regarding throughput and accuracy. Such lightweight systems typically exhibit lightly damped flexible dynamics in the controller cross-over region. State-of-the-art modeling and motion control design procedures do not deliver the required model fidelity to control the flexible dynamical behavior. In this paper, identification and control challenges are investigated and a novel approach for next-generation motion control is presented. The procedure is applied to a multivariable wafer stage, confirming a significant performance improvement.**

I. Introduction

Mass production of integrated circuits (ICs) has enabled the development of a wide variety of technologies in today's society. The state-of-the-art equipment for the automated production of ICs are wafer scanners, see Fig. 1. In the production process, the wafer must be extremely accurately positioned in six motion degrees-of-freedom (DOFs). This is the task of the wafer stage, which is the application that is considered in this paper.

In the last decades, increasing demands with respect to computing power and memory storage have led to the need for new wafer scanner technologies. Already in 1998, the replacement of deep ultraviolet (DUV) lightsources by extreme ultraviolet (EUV) lightsources was considered to be a promising technology, since it results in a reduction of the wavelength from 193 nm to 13.5 nm. Hence, smaller features can be produced on the ICs. At present, EUV constitutes a key technology in state-of-the-art wafer stages. Experimental prototypes are reported in [1] and the first production systems are presently being installed [2].

The introduction of EUV light has far-reaching consequences for all subsystems of the wafer scanner, including the wafer stage. Air absorbs the EUV light beam, hence the system has to operate in vacuum. This has important consequences for the motion control of the wafer stage.

The trends in wafer stages are expected to lead to lightweight precision motion systems for several reasons. Firstly, contactless operation is required to avoid pollution of the vacuum environment due to mechanical wear or lubricants. Secondly, market viability requires a high throughput of the wafer scanner. In view of Newton's law $F = ma$, high accelerations (a) of the system require a mass (m) reduction and hence a lightweight system is essential.

As a result of a lightweight system design, next-generation motion systems predominantly exhibit flexible dynamical behavior. On the one hand, the increasing accuracy and performance demands lead to the manifestation of flexible dynamical behavior at lower frequencies. On the other hand, due to these increasing demands, the controller has to be effective at higher frequencies. Combining these developments leads to a situation where flexible dynamical behavior is present within the control bandwidth. This is in sharp contrast to traditional positioning systems where the flexible dynamical behavior are considered as high-frequent parasitic dynamics, see [3, Sec. 2.1, Assumption 1-3]. Specific implications for motion control design include:

i) next-generation motion systems are inherently multivariable, since the flexible dynamical behavior is generally not aligned with the motion DOFs;

ii) next-generation motion systems can exploit additional actuation and sensing to deal with flexible dynamical behavior, whereas the number of inputs and outputs in the traditional situation equals the number of motion DOFs; and

Although several model-based robust control design methodologies have been developed to deal with the inherently multivariable nature of wafer stages, including [4], [3], [5], these approaches cannot deal with the model complexity that is associated with next-generation lightweight wafer stages. Indeed, robust control is essential for motion systems, since a nominal model cannot encompass the entire system behavior due to the presence of high order flexible dynamical behavior [6] and nonlinear damping effects [7]. In [4], a motion control design procedure is presented for SISO motion system that combines system identification and robust control. In [3], this approach is further extended towards multivariable systems. However, as is also argued in [3], the performance improvement is hindered by inadequacies in the system identification procedure.

The identification of accurate models in view of the control objective is of vital importance to obtain high performance robust motion control. In [5], a first step is made to intertwine the identification and control design steps. However, all the approaches in [4], [3], and [5] resort to highly structured model uncertainty structures. As a result, these approaches lead to intractable computations and unnecessary conservatism in next-generation motion control, where a high number of inputs and outputs are expected. A key consequence of the induced conservatism is that the approaches do not lead to the limit of control performance.

The key contribution of this paper is a novel framework for next-generation motion control. Hereto, system identification and robust control are connected, leading to guaranteed high performance robust motion control. The severe requirements associated with the system complexity, including the (uncertain) model complexity are explicitly addressed to obtain a computationally tractable procedure. Specifically, the following contributions are identified in this paper, leading to the following sections:

C1) *Sec. III: low-order control-relevant modeling*. In [3, Sec. 5], it is argued that new developments are essential to

Tom Oomen, Robbert van Herpen, Sander Quist, Okko Bosgra, and Maarten Steinbuch are with the Eindhoven University of Technology, Eindhoven, The Netherlands. Marc van de Wal was with Philips Applied Technologies. E-mail: t.a.e.oomen@tue.nl.

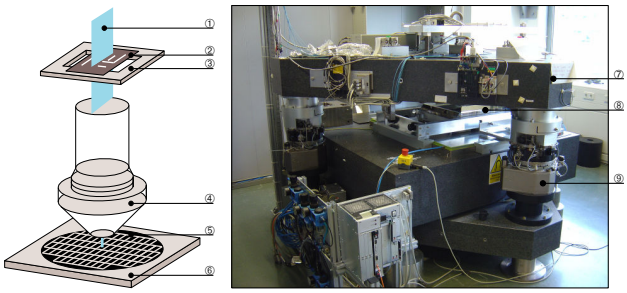

Fig. 1. Left: schematic illustration of a wafer scanner system. Right: photograph of experimental wafer stage system. ①: light source, ②: reticle, ③: reticle stage, ④: lens, ⑤: wafer, ⑥: wafer stage, ⑦: metrology frame, ⑧: mover, ⑨: airmount.

model multivariable motion systems from frequency response function data. In this paper, a new approach to obtain low-order nominal models of the wafer stage is pursued by i) directly identifying a multivariable model, thereby taking into account common dynamics in different input/output channels, and ii) only considering control-relevant dynamics, i.e., by only including dynamics in the model that will be subsequently compensated;

C2) *Sec. IV: robust-control-relevant uncertainty modeling*. Robust control is essential to guarantee stability and performance when the controller is implemented on the true system. In this paper, a new model uncertainty structure is exploited that connects the size of model uncertainty and the control criterion. On the one hand, this leads to a wafer stage model set that is tailored towards the robust control goal. On the other hand, this enables the use of unstructured perturbation models to represent the uncertainty of the wafer stage model. This is of vital importance, since the use of highly structured perturbation models, e.g., as in [3] and [5], leads to an unnecessarily high computational demand and introduced conservatism for an increasing number of inputs and outputs. In contrast, the proposed approach leads to μ-simple [8] perturbation models that facilitate nonconservative uncertainty modeling and robust control.

C3) *Sec. V: wafer stage performance improvement through robust control*. A robust controller is synthesized and implemented on the wafer stage system. This shows that the presented procedure, which is a joint procedure for system identification and robust control, significantly improves wafer stage performance, both in terms of the $\mathcal{H}_\infty$-criterion and the measured time domain results.

Furthermore, concluding remarks and relevant topics for further research are discussed in Sec. VI.

II. Problem Formulation

A. Experimental setup

The considered wafer stage system is depicted in Fig. 1. The system is equipped with a moving-coil permanent magnet planar motor that enables contactless operation. As a result, the wafer stage is suitable for operation in vacuum. Due to the contactless actuation, the motion system consists of two parts: a stator, which is a plate consisting of an ordered array of permanent magnets, and a mover, which constitutes the moving part of the wafer stage.

Four force actuators are connected to the mover, each consisting of three coils that are powered by a three-phase power source. By means of an appropriate position-dependent commutation of the coils, eight independent forces are available. Laser interferometers in conjunction with a mirror block, which are connected to the metrology frame and the wafer stage, respectively, enable a subnanometer accuracy position measurement in all six motion DOFs. Throughout, a sampling frequency of 2.5 kHz is used.

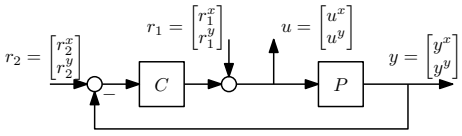

Fig. 2. Feedback configuration for wafer stage application.

The controller design in this paper is performed for the translational x and y DOFs in the horizontal plane to facilitate the exposition. It is emphasized that the presented approach is aimed to deal with a large number of actuators and sensors, possibly more than the number of motion DOFs.

B. Robust control

As is motivated in Sec. I, a model-based control design procedure is considered. Although a well-design feedforward controller is essential in servo tasks, in the present paper focus is on feedback control design. Hereto, the feedback interconnection in Fig. 2 is considered, where y is the measured position output and u is the input voltage to the amplifiers. In addition, r_2 and r_1 are external reference signals. All signals have components in both x and y directions, as is indicated by a superscript, e.g., $y = \begin{bmatrix} y^x & y^y \end{bmatrix}^T$.

The performance is quantified using the criterion

$$\mathcal{J}(P, C) = \|WT(P, C)V\|_\infty , \tag{1}$$

where W and V are weighting filters given by

$$W = \begin{bmatrix} W_y & 0 \\ 0 & W_u \end{bmatrix}, \quad V = \begin{bmatrix} V_2 & 0 \\ 0 & V_1 \end{bmatrix}, \tag{2}$$

and $T(P, C)$ is defined as

$$T(P, C) : \begin{bmatrix} r_2 \\ r_1 \end{bmatrix} \mapsto \begin{bmatrix} y \\ u \end{bmatrix} = \begin{bmatrix} P \\ I \end{bmatrix} (I + CP)^{-1} \begin{bmatrix} C & I \end{bmatrix}.$$

The use of the $\mathcal{H}_\infty$-norm in (1) has important advantages, since it enables loop-shaping-based motion controller designs [4] and enables a robust controller design.

The goal in the considered model-based control design procedure is to compute the controller C^{opt} that minimizes $\mathcal{J}(P, C))$ in (1) for the true system P_o, i.e., $C^{\text{opt}} = \arg\min_C \mathcal{J}(P_o, C))$. In this paper, P_o represents the unknown physical wafer stage system as described in Sec. II-A. Hence C^{opt} cannot be computed directly. Hereto, the knowledge regarding the true system P_o is represented by a model set $\mathcal{P}$ that encompasses the true system behavior, i.e., it satisfies

$$P_o \in \mathcal{P}. \tag{3}$$

Throughout, the model set $\mathcal{P}$ is constructed by considering a perturbation Δ_u around the nominal model $\hat{P}$, i.e.,

$$\mathcal{P} = \left\{ P \middle| P = \mathcal{F}_u(\hat{H}, \Delta_u), \Delta_u \in \mathbf{\Delta}_u \right\}. \tag{4}$$

Here, $\hat{H}$ contains the multivariable nominal model $\hat{P}$, see Sec. III, and the model uncertainty structure. In addition,

$$\mathbf{\Delta}_u = \left\{ \Delta_u \in \mathcal{RH}_\infty \middle| \|\Delta_u\|_\infty \leq \gamma, \Delta_u(e^{j\omega}) \in \mathbb{C}^{2\times 2}, \omega \in [0, 2\pi) \right\}, \tag{5}$$

i.e., an unstructured model perturbation is employed, see also Contribution C2 and Sec. IV.

Associated with $\mathcal{P}$ is the worst-case performance $\mathcal{J}_{\mathrm{WC}}(\mathcal{P}, C) = \sup_{P \in \mathcal{P}} \mathcal{J}(P, C)$. By minimizing the worst-case performance, i.e.,

$$C^{\mathrm{RP}} = \arg\min_{C} \mathcal{J}_{\mathrm{WC}}(\mathcal{P}, C), \tag{6}$$

it is guaranteed that

$$\mathcal{J}(P_o, C^{\mathrm{opt}}) \leq \mathcal{J}(P_o, C^{\mathrm{RP}}) \leq \mathcal{J}_{\mathrm{WC}}(\mathcal{P}, C^{\mathrm{RP}}), \tag{7}$$

hence C^{RP} is guaranteed to result in a certain performance when implemented on the wafer stage system, which is the essence of robust control design. In contrast, the worst-case performance for a nominal control design, i.e., $\mathcal{J}_{\mathrm{WC}}(\mathcal{P}, C^{\mathrm{NP}}(\hat{P}))$, where $C^{\mathrm{NP}} = \arg\min_C \mathcal{J}(\hat{P}, C)$, in which case the controller performs optimally for the nominal model $\hat{P}$, may even be unbounded, as is shown in Sec. V.

C. Robust-control-relevant system identification procedure

The achievable worst-case performance bound in (7) depends on the actual shape of the model set $\mathcal{P}$. Indeed, although $\mathcal{P}$ is subject to the constraint in (3), there is freedom in the choice of the nominal model $\hat{P}$ and the model uncertainty structure, see $\hat{H}$ in (4). The key question is which properties the model set $\mathcal{P}$ should have to guarantee a nonconservative control design C^{RP}, i.e., to guarantee that the worst-case performance guarantee in (7) is small.

Optimally, the identification procedure should deliver a model set such that $\mathcal{J}_{\mathrm{WC}}(\mathcal{P}, C^{\mathrm{RP}}(\mathcal{P}))$ is minimized over its argument $\mathcal{P}$, such that (3) holds. Observe that $C^{\mathrm{RP}}(\mathcal{P})$ in general depends in a complicated manner on $\mathcal{P}$, hence the use of $C^{\mathrm{RP}}(\mathcal{P})$ in an identification criterion is not directly possible. Thereto, as in [9], [10], an upper bound is employed, leading to the robust-control-relevant identification criterion

$$\min_{\mathcal{P}} \mathcal{J}_{\mathrm{WC}}(\mathcal{P}, C^{\mathrm{exp}}), \tag{8}$$
$$\text{subject to (3)}$$

Here, $\mathcal{P}$ is structured as in (4), i.e., $\mathcal{P}$ is constructed by considered a nominal model $\hat{P}$ and model uncertainty Δ_u. Also, C^{exp} is a known controller that stabilizes P_o. In fact, the wafer stage system that is considered in this paper is open-loop unstable due to a contactless operation, hence system identification has to be performed in closed-loop. In the case where C^{exp} is not sufficiently close to $C^{\mathrm{RP}}(\mathcal{P})$, then (6) and (8) may be solved iteratively, leading to a monotonous performance improvement [9]. Using the results presented in this paper, unnecessary conservatism is avoided. Hence, a large performance improvement can typically be realized in one step, rendering an iterative procedure superfluous.

The initial controller C^{exp} is a multi-loop SISO PID controller that achieves a bandwidth in terms of crossover frequency of approximately 40 Hz, see Fig. 6. The other DOFs, i.e., z-translation and three rotations, are controlled by low performance PID controllers to stabilize the system.

Furthermore, the weighting filters W and V are designed using a loop-shaping based design procedure, see [4], [3]. These weighting filters are designed using an identified *non-parametric* frequency response function of the system, which is identified prior to the estimation of a control-relevant *parameteric* model. The weighting filters are aimed at a cross-over frequency of 90 Hz.

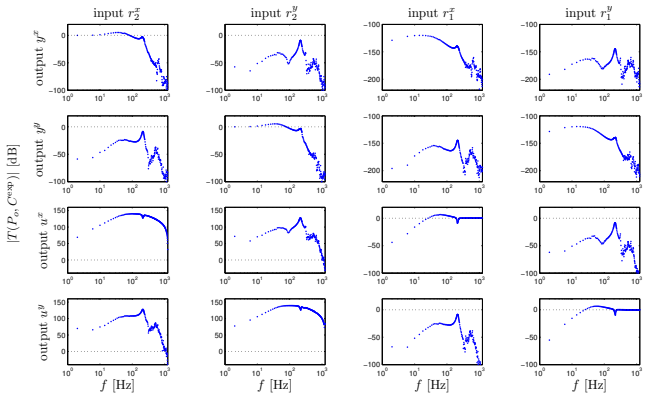

Fig. 3. Nonparametric closed-loop frequency response function estimate $\widetilde{T}(P_o, C^{\mathrm{exp}})$ for $\omega_i \in \Omega^{\mathrm{id}}$.

III. Control-relevant nominal identification

In this section, a nominal model is identified that, in conjunction with the uncertainty model in Sec. IV, provides a solution to (8). Hereto, a new connection between control-relevant system identification and coprime factor identification is employed. This leads to a new connection between the size of Δ_u and the criterion $\mathcal{J}_{\mathrm{WC}}(\mathcal{P}, C^{\mathrm{exp}})$. To relate the closed-loop performance of any candidate model and the true system, the triangle inequality is invoked, which is at the heart of common iterative identification and control techniques [11]:

$$\mathcal{J}(P_o, C) \leq \mathcal{J}(P, C) + \left\| W \left(T(P_o, C) - T(P, C) \right) V \right\|_\infty . \tag{9}$$

By evaluating (9) for the controller C^{exp} and minimizing over P, the following control-relevant identification criterion is formulated as in [11]:

$$\hat{P} = \arg\min_{P} \left\| W \left(T(P_o, C^{\mathrm{exp}}) - T(P, C^{\mathrm{exp}}) \right) V \right\|_\infty . \tag{10}$$

The control-relevant identification criterion (10) depends on the unknown system P_o. To formulate a solvable identification problem, the frequency domain interpretation of the $\mathcal{H}_\infty$-norm is exploited to recast (10) as

$$\hat{P} = \arg\min_{P} \max_{\omega_i \in \Omega^{\mathrm{id}}} \bar{\sigma} \left(W \left(\widetilde{T}(P_o, C^{\mathrm{exp}}) - T(P, C^{\mathrm{exp}}) \right) V \right) \tag{11}$$
$$\text{subject to } T(P, C^{\mathrm{exp}}) \in \mathcal{RH}_\infty$$

In (11), $\widetilde{T}(P_o, C^{\mathrm{exp}})$ represents an identified multivariable frequency response function of the wafer stage system. This frequency response function $\widetilde{T}(P_o, C^{\mathrm{exp}})$ can be identified directly using the results in [12], see Fig. 3 for the results. The optimization problem (11) is an approximation of (10). Firstly, the use of $\widetilde{T}(P_o, C^{\mathrm{exp}})$ introduces estimation errors. However, due to the use of multisine excitations and high signal-to-noise ratios, these errors are negligible. Secondly, the use of a discrete frequency grid Ω^{id} implies that (11) minimizes a lower bound of the norm in (10). To minimize potential interpolation errors, the frequency grid is chosen sufficiently dense. In addition, these interpolation errors should be part of the model uncertainty in Sec. IV.

The key step that leads towards Contribution C1-C2 involves the result of [10], which establishes that the control-relevant identification problem (11) is equivalent to

$$\min_{\hat{N}, \hat{D}} \max_{\omega_i \in \Omega^{\mathrm{id}}} \bar{\sigma} \left(W \left(\begin{bmatrix} N_o \\ D_o \end{bmatrix} - \begin{bmatrix} \hat{N} \\ \hat{D} \end{bmatrix} \right) \right) \tag{12}$$
$$\text{subject to } \hat{N}, \hat{D} \in \mathcal{RH}_\infty .$$

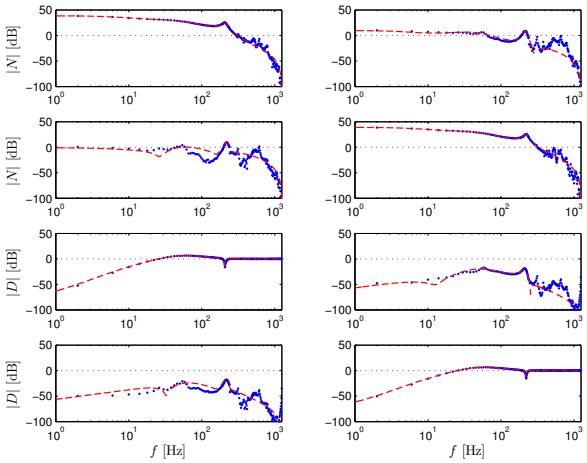

Fig. 4. Coprime factorization: nonparametric N_o, D_o (blue dots), eighth order parametric model coprime factorizations $\hat{N}$, $\hat{D}$ (dashed red).

Here, $\{\hat{N}, \hat{D}\}$ and $\{N_o, D_o\}$ are right coprime factorizations (RCFs) of $\hat{P}$ and P_o, respectively, where

$$\begin{bmatrix} N \\ D \end{bmatrix} = \begin{bmatrix} P \\ I \end{bmatrix} (\tilde{D}_e + \tilde{N}_{e,2} V_2^{-1} P)^{-1}, \tag{13}$$

and $\tilde{D}_e$ and $\tilde{N}_{e,2}$ follow from C^{exp}, V_1, V_2, see also (2), and the solution of an algebraic Riccati equation, see [10] for further details and a proof. Note that the pair $\{N, D\}$ is an RCF of P implies that [13]: i) $P = ND^{-1}$, ii) $N, D \in \mathcal{RH}_\infty$, and iii) $\exists X, Y \in \mathcal{RH}_\infty$ such that $XN + YD = I$. These coprime factorizations will turn out to have a crucial role in the construction of the uncertainty structure in Sec. IV.

The first step in solving the optimization problem (12) is determining $\{N_o, D_o\}$. Given V, C, and $\tilde{T}(P_o, C^{\text{exp}})$ for $\omega_i \in \Omega^{\text{id}}$, then N_o and D_o, see (13), can directly be computed for $\omega_i \in \Omega^{\text{id}}$, see [10], see Fig. 4.

The next step is the estimation of a parametric model $\hat{P}$ that is internally structured as a coprime factorization $\{\hat{N}, \hat{D}\}$, see (13). Hereto, a specific parametrization is used, see [10], where the underlying system model is parametrized as the nominal model is given exactly by the matrix fraction description $\hat{P}(\theta) = B(\theta)A(\theta)^{-1}$, where $B, A \in \mathbb{R}^{2\times 2}[z]$, i.e., polynomial 2×2 matrices in z. The parameterization in terms of these polynomial matrices is essential for obtaining a low-order model, see Contribution C1.

To solve the actual optimization problem (12), the iterative algorithm in [10] is employed. The results are depicted in Fig. 4 and Fig. 5.

The model order is selected using the approach presented in [14], leading to a McMillan degree equal to 8. In view of Contribution C1, the model indeed is of low order, since

i) the use of polynomial matrices, i.e., $\hat{P} = BA^{-1}$, has a direct connection to state-space models and hence provides a low-order multivariable system description. This is in sharp contrast to the models as delivered by the procedure in, e.g., [3], that does not take into account common dynamics between the different DOFs. When considering Fig. 5, observe that four states are used to model the two rigid-body modes in both the x-direction and the y-direction. The other four states are used to represent resonance phenomena. Since these resonance phenomena correspond to flexible dynamical behavior, these correspond to complex pole

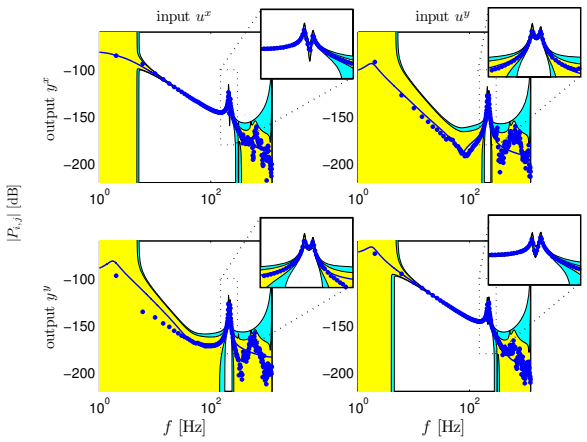

Fig. 5. Bode magnitude diagram: nonparametric estimate (dot), nominal model $\hat{P}$ (solid blue), model set $\mathcal{P}^{\text{dyn}}$ (yellow), and $\mathcal{P}^{\text{sta}}$ (cyan).

pairs. Specifically, around 208 Hz and 214 Hz two closely spaced resonance phenomena are present. Interestingly, these resonance phenomena correspond to inherently multivariable behavior, since both these resonances appear in all four transfer functions in Fig. 5, yet only require two orders each.

ii) the low-order model is obtained stems from the control-relevant identification criterion (12) that emphasizes dynamics that are especially relevant for control. The coprime factor domain in Fig. 4 directly connects to control-relevance in terms of (10). Indeed, system dynamics that have a high gain in the coprime factor domain are important for control and should be modeled accurately, which is clearly the case in Fig. 4. This is further supported by the results in Sec. IV.

IV. Identification for Robust Control

Since the nominal model $\hat{P}$ is not exact, the model quality is taken into account during robust control design by means of an uncertainty model. The key contribution, see C2, involves the construction of an uncertainty model that, in conjunction with the nominal model of Sec. III, addresses the identification problem (8). The main ingredient involves the specific coprime factorization in (12).

A. Robust-control-relevant model uncertainty structure

The coprime factorization resulting from (12) is used to generate candidate models

$$P = (\hat{N} + D_c\Delta_u)(\hat{D} - N_c\Delta_u)^{-1},\ \Delta_u \in \mathbf{\Delta}_u \subset \mathcal{RH}_\infty, \tag{14}$$

where a specific, (W_u,W_y)-normalized coprime factorization of C^{exp} is used, see [10].

To illustrate the advantages of this specific robust-control-relevant uncertainty structure (14), observe that for many uncertainty structures, including additive uncertainty [13], the performance under closed-loop with C^{exp} is given by

$$\mathcal{J}(P, C^{\text{exp}}) = \|\hat{M}_{22} + \hat{M}_{21}\Delta_u(I - \hat{M}_{11}\Delta_u)^{-1}\hat{M}_{12}\|_\infty,$$

see [10] for details. In general, $\hat{M}_{11} \neq 0$, hence $\mathcal{J}(P, C^{\text{exp}})$ can become unbounded for some Δ_u in a bounded set $\mathbf{\Delta}_u$. For the model uncertainty structure (14) for *any* right coprime factorization of $\hat{P}$ and C^{exp}, the performance is given by

$$\mathcal{J}(P, C^{\text{exp}}) = \|\hat{M}_{22} + \hat{M}_{21}\Delta_u\hat{M}_{12}\|_\infty,$$

in which case a norm-bounded Δ_u always leads to a bounded criterion value. However, the criterion can become arbitrarily

large, since $\hat{M}_{21}$ and $\hat{M}_{12}$ are multivariable and frequency-dependent functions.

The specific coprime factorization $\{\hat{N}, \hat{D}\}$ of $\hat{P}$ that is identified in Sec. III, in conjunction with a specific (W_u, W_y)-normalized coprime factorization of $C^{\rm exp}$, see [10] for a state-space computational procedure, leads to the following stronger bound on the worst-case performance

$$\mathcal{J}_{\rm WC} \leq \mathcal{J}(\hat{P}, C^{\rm exp}) + \gamma, \tag{15}$$

where γ is defined in (5). See [10] for a proof.

The bound (15) is an important and significant extension of identification-related uncertainty structures for robust control and involves Contribution C2 of this paper. Indeed, it transparently connects the size of *unstructured* model uncertainty and the control criterion by appropriately scaling the model uncertainty channels with respect to the control criterion. As a result, unstructured model uncertainty can be used without unnecessarily introducing conservatism. This is in sharp contrast to earlier approaches, including [3] and [5].

B. Size of model uncertainty

The model uncertainty structure (14) leads to the important result (15). Hence, it remains to estimate the size γ such that the constraint (3) holds. Hereto, the validation-based uncertainty modeling procedure that is presented in detail in [15] is employed. The result of the validation procedure is a static bound $\gamma = 2.1$ on the model uncertainty, leading to a model set $\mathcal{P}^{\rm sta}$. In addition, a dynamic overbound is used, that reduces the potential conservatism in the approach, as is explained in [14]. This leads to a model set $\mathcal{P}^{\rm dyn} \subset \mathcal{P}^{\rm sta}$.

By using the procedure that is presented in detail in [16], the resulting uncertain model sets $\mathcal{P}^{\rm sta}$ and $\mathcal{P}^{\rm dyn}$ are visualized in Fig. 5. The Bode diagrams corresponding to $\mathcal{P}^{\rm sta}$ best illustrate robust-control-relevance in the sense of (8) and (15) and reveal that those phenomena that are important for subsequent control are contained in the identified model set with high fidelity. Specifically, it is observed that the two resonance phenomena around 200 Hz are very accurately modeled. Interestingly, the rigid-body behavior is accurately modeled around the desired closed-loop bandwidth of 90 Hz. However, at low frequencies, where the rigid-body mode dominates the system behavior, the model set is relatively large and hence uncertain. A similar observation holds at higher frequencies, where the model set increases for increasing frequencies. Thus, from a control perspective, there is no significant benefit from explicitly modeling the high frequent resonance phenomena in $\hat{P}$, at least in terms of the target closed-loop bandwidth of 90 Hz. Observe that the shape of this model set is principally different from those obtained by alternative model uncertainty structures, including additive and multiplicative uncertainty. Finally, observe from Fig. 5 that indeed $\mathcal{P}^{\rm dyn} \subset \mathcal{P}^{\rm sta}$.

V. Robust Controller Design and Implementation

In this section, the identified model set $\mathcal{P}^{\rm dyn}$ in Sec. III and Sec. IV is used as a basis for robust controller synthesis. The optimal controller is then implemented on the true system.

Firstly, the actual robust controller synthesis (6) is solved through a skewed structured singular value synthesis. Hereto, $D-K$-iterations are generalized to take the skewness into account. Interestingly, the considered uncertainty structure

TABLE I

Identification and Controller Synthesis Results.

Controller	Minimized criterion	$\mathcal{J}(\hat{P}, C)$	$\mathcal{J}_{\rm WC}(\mathcal{P}^{\rm sta}, C)$	$\mathcal{J}_{\rm WC}(\mathcal{P}^{\rm dyn}, C)$
$C^{\rm exp}$	None (PID)	89.91	92.05	90.16
$C^{\rm NP}$	$\mathcal{J}(\hat{P}, C)$	10.94	∞	∞
$C^{\rm RP}$	$\mathcal{J}_{\rm WC}(\mathcal{P}^{\rm dyn}, C)$	16.38	∞	16.43

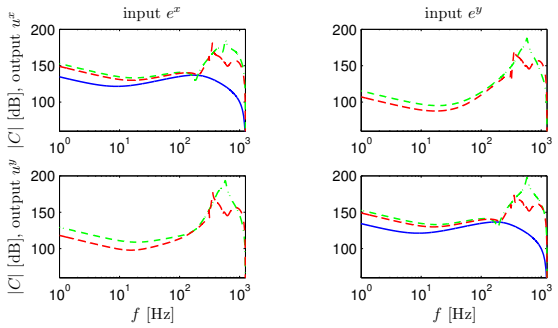

Fig. 6. Bode magnitude diagram: initial controller $C^{\rm exp}$ (solid blue), $C^{\rm RP}$ (dashed red), $C^{\rm NP}$ (dash-dotted green).

associated with the considered synthesis problem is μ-simple, see [8, Sec. 9]. Consequently, the use of upper bounds in $D-K$-iterations leads to exact results and does not introduce any conservatism. In contrast, when the number of perturbation blocks in $\mathbf{\Delta}_u$ exceeds 2, as is the case in the approaches in [3] and [5], then the use of upper bounds for the structured singular value for robust performance synthesis, as is done in typical $D-K$-iterations, introduces conservatism. Secondly, for comparison, also a nominal controller $C^{\rm NP}$ is synthesized using $\hat{P}$ and standard $\mathcal{H}_\infty$-optimization.

The resulting controllers are depicted in Fig. 6, whereas their performance is given in Table I. Here, ∞ implies absence of robust stability. Several observations are made.

i) The controller $C^{\rm NP}$ achieves optimal performance for the nominal model $\hat{P}$, i.e., $\mathcal{J}(\hat{P}, C^{\rm NP}) = 10.94$. However, the worst-case performance associated with $\mathcal{P}^{\rm dyn}$ is unbounded, hence neither stability nor performance can be guaranteed when implementing $C^{\rm NP}$ on the true system P_o. This underlines the necessity of a robust control design.

ii) The controller $C^{\rm RP}$ achieves optimal worst-case performance for the model set $\mathcal{P}^{\rm dyn}$. Indeed, the bounds

$$\mathcal{J}_{\rm WC}(\mathcal{P}^{\rm dyn}, C^{\rm RP}) \leq \mathcal{J}_{\rm WC}(\mathcal{P}^{\rm dyn}, C^{\rm exp})$$
$$\mathcal{J}_{\rm WC}(\mathcal{P}^{\rm dyn}, C^{\rm RP}) \leq \mathcal{J}_{\rm WC}(\mathcal{P}^{\rm dyn}, C^{\rm NP})$$

hold as is expected. In addition, $\mathcal{J}_{\rm WC}(\mathcal{P}^{\rm dyn}, C^{\rm RP})$ is significantly lower than $\mathcal{J}_{\rm WC}(\mathcal{P}^{\rm dyn}, C^{\rm exp})$, hence the controller $C^{\rm RP}$ leads to significantly improved performance.

iii) In contrast to the initial controller $C^{\rm exp}$, the optimal controllers $C^{\rm NP}$ and $C^{\rm RP}$ are inherently multivariable. Indeed, the inputs and outputs of the wafer stage system have equal units and comparable magnitude. Next, in Fig. 6 it is observed that the off-diagonal elements have a comparable magnitude to the diagonal elements in the high frequency range. Clearly, the compensation of the inherently multivariable resonance phenomena benefits from a multivariable controller.

Next, the controllers $C^{\rm exp}$ and $C^{\rm RP}$ are implemented on the true wafer stage system. The controller $C^{\rm NP}$ is not implemented, since it potentially destabilizes the system, see also Table I. The evaluation of standstill errors is an important performance indicator for wafer stage systems. Here, the reference signal is set to zero, leading to a regulator

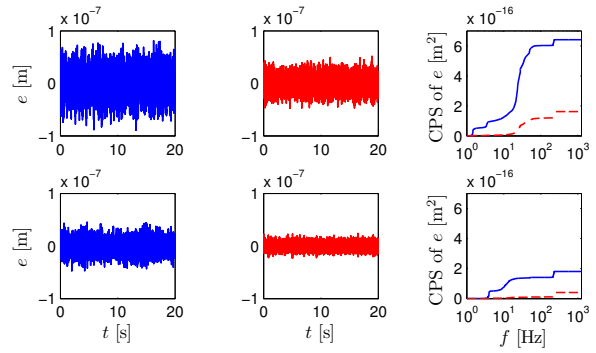

Fig. 7. Measured error signals in x-direction (top) and y-direction (bottom). Left: initial controller C^{exp}. Middle: robust controller C^{RP}. Right: cumulative power spectrum of the measured error signal with C^{exp} (solid blue) and C^{RP} (dashed red).

TABLE II

STANDARD DEVIATION AND PEAK ERROR SIGNALS IN [NM].

	σ^x	σ^y	p^x	p^y
C^{exp}	25.3	13.5	129.4	60.4
C_8^{RP}	12.7	6.4	54.1	27.4

problem with performance variable $e = -y$. In this case, the key task of the feedback controller is to attenuate exogenous disturbances that affect the wafer stage.

The resulting time domain measurements are depicted in Fig. 7, whereas the cumulative power spectrum (CPS) is depicted in Fig. 7. The standard deviation σ^x and σ^y and peak values p^x and p^y for the x-direction and y-direction, respectively, are given in Table II. These results confirm that C^{RP} leads to significantly improved performance.

VI. CONCLUSIONS

In this paper, a combined system identification and robust control framework is presented for next-generation motion control. The approach provides new, computationally tractable techniques for accurate identification and uncertainty modeling for mechanical systems with high order flexible dynamics and many inputs and outputs. Application to an industrial wafer stage reveals a significant and guaranteed performance improvement through a systematic procedure.

The key technical result that enables the developments in this paper is a new coprime factorization. On the one hand, a new connection between coprime factor identification and control-relevant identification leads to a low order nominal model. On the other hand, a new connection between the size of model uncertainty and the control criterion enables the non-conservative use of unstructured uncertainty. As a result, a robust-control-relevant model set is obtained that is of low complexity, facilitating a robust controller synthesis.

VII. EXTENSIONS

Continued research topics that are beyond the scope of the present paper includes the following aspects.

- Dealing with unmeasured performance variables [17].
- Dealing with position-dependent dynamics. Motion systems involve moving parts of the system, hence the dynamics may depend on operating conditions. Although an initial attempt to improve the control performance through position-dependent wafer stage modeling is presented in [18], the resulting position-dependent controller does not significantly improve the performance. An explanation for the lack of performance improvement is the fact that the identified position-dependent models in [18] are not aimed towards the control goal. Indeed, in [19, Sec. 5.7], the position-dependency of the wafer stage dynamics is investigated from a control perspective using the results of Sec. IV of the present paper, revealing that the changing dynamics are irrelevant from a robust control perspective. These observations motivate the need for *control-relevant* system identification techniques for position-dependent dynamics.
- Extension of the control goal definition. Hereto, the loop-shaping techniques in the present paper should be extended towards incorporating models of the disturbances that affect the wafer stage system, see, e.g., Fig. 7.
- The investigation of the limits of achievable control performance for the traditional motion control situation, where the number of inputs and outputs equals the number of motion DOFs. Next, performance may be improved when additional actuators and sensors are placed.

REFERENCES

[1] G. D. Hutcheson, "The first nanochips," *Scient. Americ.*, pp. 48–55, April 2004.

[2] S. Adee, "EUV's underdog light source will have its day," *IEEE Spectrum*, vol. 47, no. 11, pp. 13–14, 2010.

[3] M. van de Wal, G. van Baars, F. Sperling, and O. Bosgra, "Multivariable $\mathcal{H}_\infty/\mu$ feedback control design for high-precision wafer stage motion," *Contr. Eng. Prac.*, vol. 10, no. 7, pp. 739–755, 2002.

[4] M. Steinbuch and M. L. Norg, "Advanced motion control: An industrial perspective," *Eur. J. Contr.*, vol. 4, no. 4, pp. 278–293, 1998.

[5] R. A. de Callafon and P. M. J. Van den Hof, "Multivariable feedback relevant system identification of a wafer stepper system," *IEEE Trans. Contr. Syst. Techn.*, vol. 9, no. 2, pp. 381–390, 2001.

[6] P. C. Hughes, "Space structure vibration modes: How many exist? Which ones are important?" *IEEE Contr. Syst. Mag.*, vol. 7, no. 1, pp. 22–28, 1987.

[7] R. S. Smith, "Closed-loop identification of flexible structures: An experimental example," *J. Guid., Contr., Dyn.*, vol. 21, no. 3, pp. 435–440, 1998.

[8] A. Packard and J. Doyle, "The complex structured singular value," *Automatica*, vol. 29, no. 1, pp. 71–109, 1993.

[9] R. A. de Callafon and P. M. J. Van den Hof, "Suboptimal feedback control by a scheme of iterative identification and control design," *Math. Mod. Syst.*, vol. 3, no. 1, pp. 77–101, 1997.

[10] T. Oomen and O. Bosgra, "System identification for achieving robust performance," *Accepted for publication in Automatica*, 2012.

[11] R. J. P. Schrama, "Accurate identification for control: The necessity of an iterative scheme," *IEEE Trans. Automat. Contr.*, vol. 37, no. 7, pp. 991–994, 1992.

[12] R. Pintelon and J. Schoukens, *System Identification: A Frequency Domain Approach*. New York, NY, USA: IEEE Press, 2001.

[13] S. Skogestad and I. Postlethwaite, *Multivariable Feedback Control: Analysis and Design*, 2nd ed. West Sussex, UK: John Wiley & Sons, 2005.

[14] R. van Herpen, T. Oomen, and O. Bosgra, "A robust-control-relevant perspective on model order selection," in *Proc. 2011 Americ. Contr. Conf.*, San Francisco, CA, USA, 2011, pp. 1224–1229.

[15] T. Oomen and O. Bosgra, "Well-posed model uncertainty estimation by design of validation experiments," in *15th IFAC Symp. Sys. Id.*, Saint-Malo, France, 2009, pp. 1199–1204.

[16] T. Oomen, S. Quist, R. van Herpen, and O. Bosgra, "Identification and visualization of robust-control-relevant model sets with application to an industrial wafer stage," in *Proc. 49th Conf. Dec. Contr.*, Atlanta, GA, USA, 2010, pp. 5530–5535.

[17] T. Oomen, E. Grassens, F. Hendriks, R. van Herpen, and O. H. Bosgra, "Inferential motion control: Identification and robust control with unmeasured performance variables," in *Proc. 50th Conf. Dec. Contr.*, Orlando, FL, USA, 2011.

[18] M. Groot Wassink, M. van de Wal, C. Scherer, and O. Bosgra, "LPV control for a wafer stage: Beyond the theoretical solution," *Contr. Eng. Prac.*, vol. 13, pp. 231–245, 2003.

[19] T. Oomen, "System identification for robust and inferential control with applications to ILC and precision motion systems," Ph.D. dissertation, Eindhoven University of Technology, Eindhoven, The Netherlands, 2010.